JACS
JOURNAL OF THE AMERICAN CHEMICAL SOCIETY
pubs.acs.org/JACS
Article

3D-Shaped Binders of Unfolded Proteins Inducing Cancer Cell-Specific Endoplasmic Reticulum Stress In Vitro and In Vivo

Insa Klemt, Oleg Varzatskii, Roman Selin, Serhii Vakarov, Vladyslava Kovalska, Galyna Bila, Rostyslav Bilyy, Yan Voloshin, Itziar Cossío Cuartero, Andrés Hidalgo, Benjamin Frey, Ina Becker, Bernhard Friedrich, Rainer Tietze, Ralf P. Friedrich, Christoph Alexiou, Elena-Laura Ursu, Alexandru Rotaru, Iris Solymosi, M. Eugenia Pérez-Ojeda, and Andriy Mokhir*

Cite This: https://doi.org/10.1021/jacs.3c08827
Read Online

ABSTRACT: The amount of unfolded proteins is increased in cancer cells, leading to endoplasmic reticulum (ER) stress. Therefore, cancer cells are sensitive to drugs capable of further enhancing ER stress. Examples of such drugs include the clinically approved proteosome inhibitors bortezomib and carfilzomib. Unfortunately, the known ER stress inducers exhibit dose-limiting side effects that justify the search for better, more cancer-specific drugs of this type. Herein, we report on FeC **2**, which binds to unfolded proteins prevents their further processing, thereby leading to ER stress and ROS increase in cancer cells, but not in normal cells. FeC **2** exhibits low micromolar toxicity toward human acute promyelocytic leukemia HL-60, Burkitt's lymphoma BL-2, T-cell leukemia Jurkat, ovarian carcinoma A2780, lung cancer SK-MES-1, and murine lung cancer LLC1 cells. Due to the cancer-specific mode of action, **2** is not toxic in vivo up to the dose of 147 mg/kg, does not affect normal blood and bone marrow cells at the therapeutically active dose, but strongly suppresses both primary tumor growth (confirmed in Nemeth-Kellner lymphoma and LLC1 lung cancer models of murine tumor) and spreading of metastases (LLC1).

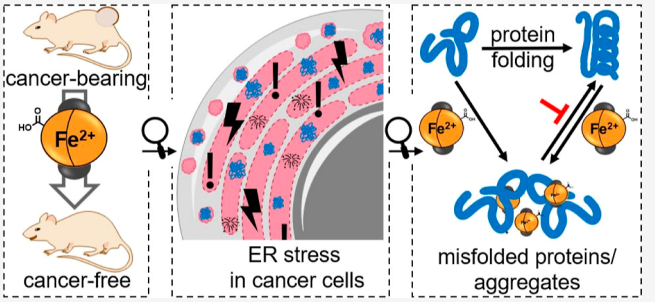

INTRODUCTION

Chemotherapy is an established method of cancer treatment. It explores different sensitivities of cancer and normal cells to some chemotherapeutic agents. For example, drugs binding to DNA (Pt^{2+} complexes, alkylating agents, and intercalators) or to DNA-binding proteins (camptothecin and its derivatives) affecting topoisomerase I and drugs inducing DNA modification (antimetabolites) all disturb replication and transcription, thereby affecting rapidly dividing cancer cells stronger than normal cells.[1] Another prominent feature of many types of cancer cells is the increased protein misfolding, leading to accumulation of unfolded proteins (UPs). The UPs contribute to the heightened level of endoplasmic reticulum (ER) stress that causes the upregulated UP response (UPR) (Figure 1A).[2]

The already stressed cancer cells are highly responsive to drugs able to further amplify the ER stress that has been explored in cancer therapy. In particular, proteasome inhibitors bortezomib[3] and carfilzomib[4] have been approved both in the United States and the EU for the treatment of multiple myeloma. Unfortunately, these drugs are not fully cell specific. They affect normal cells leading to dose-limiting neutropenia and thrombocytopenia, gastrointestinal effects, and peripheral neuropathy,[3,4] which justifies the search for the less toxic drugs.

Metallodrugs are emerging as alternative ER stress inducers.[2b,5] Compared to organic drugs, they offer additional metal-centered reactivity for drug design including coordination chemistry, photo(redox) chemistry, and dark redox chemistry. The metallodrugs can trigger the ER stress via four distinct upstream events.[2b,5] First, coordinatively unsaturated complexes (CUCs) form metal−biomolecule bonds, e.g., Pt^{2+} in cisplatin binds N7 of purine residues in DNA,[6] Au^{+} complexes coordinate a selenocysteine residue in thioredoxin reductase,[7] Ir^{3+} half-sandwich complexes bind histidine and cysteine residues in proteins,[8] and a Ru^{3+} complex BOLD-100/KP1339 binds ribosomal proteins.[9] Second, redox-active complexes induce the catalytic generation of reactive products via electron transfer either to or from intracellular substrates. Representatives of the complexes of the former type are polypyridyl complexes of Ru^{2+} and aminoferrocene prodrugs,[10]

Received: August 14, 2023

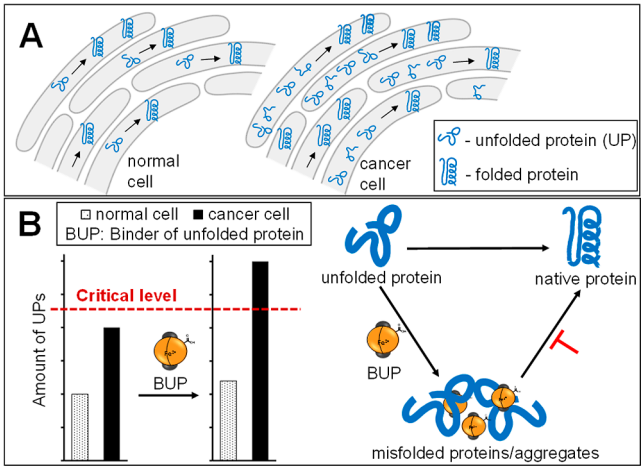

Figure 1. (A) Illustration of a hallmark of cancer cells: a higher intracellular amount of UPs and enhanced ER stress. (B) Approach to selectively kill cancer cells by inducing the ER stress by a binder of UPs (BUP). The critical level of the ER stress is indicated with a red line.

which catalyze generation of reactive oxygen species (ROS) $O_2^{\bullet-}$ and HO• from O_2 and H_2O_2, respectively. A representative of the complexes of the latter type is the half-sandwich Ru^{2+} arene complex, which catalyzes oxidation of glutathione (GSH) to GSSG.[11] Third, metal complexes induce generation of toxic products via photoinduced energy or electron transfers, e.g., VO^{2+}, bimetallic Cu^{+}–Fe^{2+}, and Ir^{3+} complexes,[12−14] all act as photosensitizers by generating ROS including either $^1O_2$ or $O_2^{\bullet-}$ or both of them. Fourth, positively charged lipophilic compounds, e.g., cyclometalated Ir^{3+} complexes,[15] are accumulated in the negatively charged membrane of mitochondria (Mit) causing Mit dysfunction and ROS production. In all of these cases, either coordination of CUCs to nucleophilic sites of biological macromolecules or direct or indirect intracellular ROS generation or both take place not only in cancer but also in normal cells, which leads to undesired toxicity.

In search of alternative ER stress inducers, which are not CUCs and do not cause systemic ROS production, we were drawn to binders of UPs (BUPs). These could stabilize UPs, eventually leading to their accumulation or/and aggregation, thereby inducing the ER stress (Figure 1B). The interaction of BUP and UPs is at least a bimolecular reaction. As such, it is strongly dependent on concentrations of both BUP and UPs. In cancer cells containing the high level of UPs, the equilibrium BUP + UPs → BUP/UPs is shifted to the BUP/UPs, leading to ER stress. In contrast, in normal cells containing the low level of UPs, this equilibrium is shifted toward the unbound UPs, which can be normally processed. Thus, the optimized BUP will be toxic to cancer cells, but not affect normal cells (Figure 1B), thereby solving the problem of side effects of common ER stress inducers.[3−15]

Several synthetic binders of UPs have been identified previously, e.g., chemical chaperones 4-phenylbutyrate and lysophosphatidic acids[16] as well as a molecular tweezer CLR01.[17] In contrast to the suggested BUPs, they reduce the intracellular load of UPs, thereby attenuating rather than enhancing the ER stress.[18] Correspondingly, the anticancer activity of these compounds is low.[19] Another potential BUP is the carbon allotrope fullerene C_{60}. Though it is known to bind strongly UPs,[20] medicinal applications of C_{60} are limited by its poor solubility in water (log S = −11.0[21]). A better water-soluble metal-containing carbon allotrope Gd-$C_{82}(OH)_{22}$ exhibits moderate anticancer activity.[22] However, its mode of action is not related to binding UPs. We have previously prepared and studied Fe-clathrochelates (FeCs), which are coordination compounds with a 3D-shaped structure having dimensions similar to that of C_{60} (Scheme 1).[23] We have found that, similarly to C_{60}, the FeCs functionalized with either six (Vz375,[24] Scheme S1, Supporting Information) or two carboxylic acid moieties (FeC **1**,[25] Scheme 1) bind to model UPs. Their anticancer activity has not been studied before. Compared to C_{60}, FeCs exhibit several favorable properties. In particular, as less hydrophobic compounds, the FeCs are more water soluble (e.g., log S = −4.4 for FeC **2**, Scheme 1). Furthermore, in contrast to C_{60}, they are not redox active at physiological conditions and therefore are not expected to directly generate ROS or other toxic reactive species that could adversely affect normal cells. Importantly, chemical modification of the exterior of FeCs is straightforward and can be achieved by the variation of the substituents of the dioxime ligands and boron-containing cap groups that allows fine-tuning of the properties of FeCs for medicinal applications.[23] All of the factors mentioned above make FeCs a suitable scaffold for the development of the BUPs. A single previously reported FeCs exhibiting some anticancer activity is electrophilic FeC_Cl_6 (Scheme S1, Supporting Information).[26] The latter compound alkylates intracellular glutathione (GSH), leading to the ROS increase in both cancer and normal cells and, therefore, is not suitable for further development as a drug.

Scheme 1. Structures and Some Properties of Drugs/Controls FeCs 1−5 and C_{60}[21]

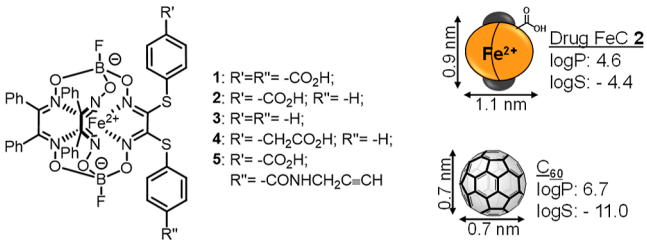

In this paper, we report on optimized BUP FeC **2**. It binds model UPs, induces the ER stress, as well as increases the levels of mitochondrial ROS and nitric oxide (NO) in cancer cells. In contrast, it does not affect normal cells. Further, the FeC is nontoxic in vivo up to a dose of 147 mg/kg and exhibits strong anticancer and antimetastatic activities in three murine models of cancer.

RESULTS AND DISCUSSION

Preliminary Studies, Synthesis, and Properties of the Selected FeCs in Cell-Free Settings. Though previously reported Vz375[24] and **1**[25] bind UPs, they are either inactive (Vz375, half-maximal inhibitory concentration (IC_{50}) > 50 μM for human ovarian carcinoma A2780 cells) or exhibit weak anticancer activity toward a range of cancer cell lines: the IC_{50} value of **1** for human acute promyelocytic leukemia HL-60, A2780, Burkitt's lymphoma BL-2, T-cell leukemia Jurkat, and lung cancer SK-MES-1 cells is >32 μM, whereas the IC_{50} value for murine lung cancer LLC1 cells is >15 μM (Table 1).

https://doi.org/10.1021/jacs.3c08827
J. Am. Chem. Soc. XXXX, XXX, XXX−XXX

Table 1. Effects of FeCs on the Viability of Selected Cancer Cell Lines[a]

	IC_{50} (μM)[d] for cell lines					
FeC	HL-60	A2780	BL-2	Jurkat	SK-MES1	LLC1
1	40 ± 2	40 ± 1	32 ± 5	>50[b]	43 ± 3	>15[c]
2	1.3 ± 0.3	2.6 ± 0.6	0.6 ± 0.1	3 ± 1[b]	21 ± 2	12.0 ± 0.4[c]
4		2.9 ± 0.2				
5		4.7 ± 0.0				

[a]The cells were incubated with the compounds for 48 h, except of data indicated with. [b](24 h) and. [c](72 h). FeC = clathrochelate. [d]IC_{50}: half-maximal inhibitory concentration.

Since these FeCs are relatively polar due to the presence of six (Vz375) or two (**1**) carboxylic acid groups, their low activity could be caused by the inefficient membrane permeability. To determine whether this is the case, we investigated the uptake of one of these compounds in BL-2 cells. By using atomic emission spectroscopy (AES), we observed no statistically significant increase of the intracellular amount of both iron and boron in BL-2 cells incubated for 4 h with **1** (9 μM) as compared to untreated BL-2 cells (Figure 2A).

These data confirm that the uptake of FeC **1** by BL-2 cells is poor. In search for membrane-permeable FeCs, we explored potentially more lipophilic compounds containing one (**2**) or no carboxylic acids (**3**[27]) (Scheme 1). The previously unknown FeC **2** was prepared starting from the electrophilic FeC intermediate **S1** by the nucleophilic substitution reaction using thiophenol in the presence of triethylamine (NEt_3) as described in the Supporting Information. To evaluate the lipophilicity of FeCs **2** and **3**, we determined their *n*-octanol/water partition coefficients (log *P*'s, Table S1, Supporting Information). As expected, both compounds (log *P*(**2**) = 4.6 ± 0.2 and log *P*(**3**) = 5.6 ± 0.3) are more lipophilic than the reference FeC **1** (log *P* = 3.7 ± 0.1). Importantly, despite its higher lipophilicity, the solubility of FeCs **2** in aqueous solutions is still sufficient for the studies of its biological activity: 40 ± 8 μM in aqueous phosphate-buffered saline (PBS) solution and 74 ± 10 μM in Roswell Park Memorial Institute 1640 (RPMI 1640) medium containing fetal bovine serum (FBS, 5%), L-glutamine (Gln, 1%), and penicillin/streptomycin (1%) (Table S2, Supporting Information). In contrast, FeC **3** is insoluble at >10 μM in the aqueous solutions that precluded its further tests. All further studies focused on FeC **2** and its analogues **4** and **5**.

Anticancer Effects, the Active Form of FeC 2. The reference FeC **1** is weakly toxic toward several human and murine cancer cell lines originating from blood (HL-60, BL-2, Jurkat), ovary (A2780), and lungs (SK-MES1, LLC1). We tested the effects of FeC **2** on the same set of cells to be able to compare the anticancer efficacies of **2** and reference **1**. We found that FeC **2** is a substantially more potent anticancer agent than **1**, affecting cell viability at IC_{50} ranging from 0.6 μM for the most sensitive BL-2 cells to 21 μM for the least sensitive SK-MES1 cells (Table 1). These data show that the presence of one rather than two or six CO_2H groups is required for the anticancer activity of FeC. We conducted further in vitro studies mostly with A2780 cells as a representative cancer cell line. In few cases, the same experiments were also done for BL-2 cells to confirm that the effects observed are not restricted to a single cell line.

To find out whether it is critical for the activity that the CO_2H group is directly attached to the phenyl ring, we prepared an analogue FeC **4** containing a methylene bridge between the phenyl ring and the CO_2H group. This compound was obtained in two steps (Supporting Information). First, the nucleophilic substitution reaction between the electrophilic intermediate **S2** and 2-(4-mercaptophenyl)acetic acid in the presence of NEt_3 furnished intermediate **S3**. Second, **S3** was reacted with thiophenol in the presence of NEt_3 to obtain FeC **4**. We found that the anticancer efficacy of FeC **4** in A2780 cells (IC_{50} = 2.6 ± 0.6 μM) is identical to that of FeC **2** (IC_{50} = 2.9 ± 0.2 μM, Student's *t*-test, $p > 0.05$). These data might

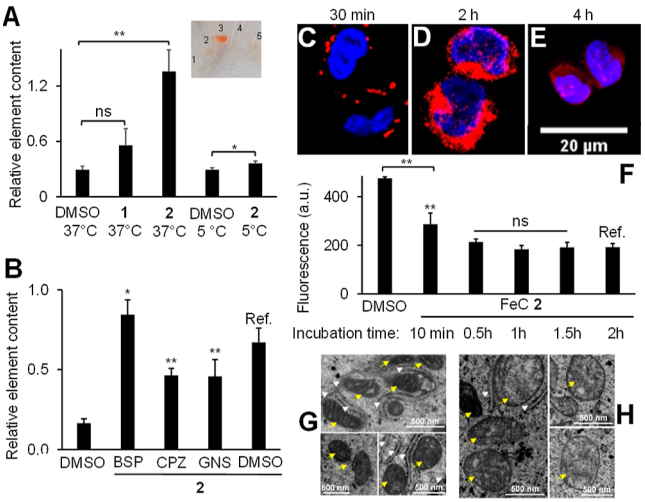

Figure 2. (A) Uptake of FeCs **1** and **2** (each 9 μM, incubation: 4 h) in BL-2 cells at 37 or 5 °C by monitoring intracellular iron content (data on the boron content: Figure S16, Supporting Information). Inset: a photo of BL-2 cells incubated with FeC or controls (orange color indicates accumulation of FeCs): (1) DMSO, 37 °C; (2) FeC **1**, 37 °C; (3) FeC **2**, 37 °C; (4) DMSO, 5 °C; and (5) FeC **2**, 5 °C. (B) Cells were pretreated with the OAT inhibitor bromsulfthalein (BSP, 500 μM, 5 min preincubation), with the clathrin-mediated uptake inhibitor chlorpromazine (CPZ. Ten μg/mL, 2 h preincubation) or with the caveolin-mediated uptake inhibitor genistein (GNS, 400 μM). After the preincubation, the cells were treated with FeC **2** for 2 h in the medium at 37 °C. The uptake was evaluated by determination of intracellular iron amount. (C–E) Visualization of the intracellular distribution of FeC **5** (9 μM) in A2780 cells after 0.5, 2, and 4 h incubation. FeC was labeled by Alexa Fluor 594 Azide. The nuclei of the cells were costained with Hoechst 33342. Ch1 (red)—λ_{ex}: 561 nm; λ_{em}: 595 ± 50 nm; Ch2 (blue)—λ_{ex}: 355 nm; and λ_{em}: 450 ± 50 nm. (F) Effects of the time of FeC **2** (9 μM) incubation with A2780 cells (10 min–2 h) on ER-specific staining of the cells. After the cells were incubated with the FeC for the specified time, the ER probe was added, and the cells were incubated for an additional 20 min (Supporting Information). For (A,B,F), unpaired Student's *t*-test *: $p < 0.05$; **: $p < 0.01$; ***: $p < 0.001$; ns > 0.05. (G,H) TEM images of A2780 cells. (G) Control (no FeC added). (H) FeC **2** (9 μM), preincubation for 4 h. White arrowheads indicate ER, and yellow arrows indicate mitochondria (Mit).

https://doi.org/10.1021/jacs.3c08827
J. Am. Chem. Soc. XXXX, XXX, XXX−XXX

indicate that the binding sites of **2** and **4** in their putative target can tolerate at least small structural changes that would be in agreement with binding to unstructured UPs. The latter conclusion is further supported by the fact that FeC **5**,[28,29] containing a larger propargylaminocarbonyl moiety in the para-position of one of the phenyl residues, is only slightly less active than its analogue **2**: IC_{50} = 4.7 ± 0.0 μM versus 2.6 ± 0.6 μM, correspondingly (Table 1). We used FeC **5** for the study of the intracellular distribution of FeCs as described below.

Lipophilic drugs can form aggregates in aqueous solutions, which may destabilize the protein structure, leading to their unfolding, thereby causing both cell- and target-unspecific toxicity.[30] To exclude this possibility, we investigated whether FeC **2** forms aggregates by using UV−visible spectroscopy and dynamic light scattering (DLS). We observed that the absorbance at 487 nm (A_{max}) of solutions of **2** in aqueous PBS (pH 7.4) is linearly dependent on the compound concentration up to at least 30 μM (R^2 = 0.9986, Figure S10, Supporting Information), indicating that only one species exists in this concentration range. Further, we did not detect aggregated species in aqueous solutions of FeC **2** at <30 μM by using DLS. These data indicate that **2** exists in the monomeric form in aqueous solutions at <30 μM concentrations. Since IC_{50} values for the tested cancer cell lines are also <30 μM (Table 1), we conclude that the monomeric form rather than the aggregates is responsible for the anticancer activity of the FeC.

A single previously described clathrochelate exhibiting strong anticancer activity is an electrophilic derivative FeC_Cl6 (Scheme S1, Supporting Information). Its mode of action relies on the covalent modification of GSH via the nucleophilic substitution of the chlorides in the FeC.[26] Potentially, FeC **2** could exhibit similar chemical reactivity via the substitution of a PhS^- moiety with GS^- derived from GSH. It is a less likely reaction because PhS^- is not as good leaving group as Cl^-. However, in cancer cells, the latter reaction can be facilitated by the follow-up oxidation of PhS^- to PhSSPh, thereby shifting the equilibrium toward the product. By using LC−MS (Figure S11, Supporting Information) as well as by monitoring the release of free Fe^{2+} and Fe^{3+} ions (Table S3, Supporting Information), we confirmed that FeC **2** is chemically stable both in the absence and presence of GSH. We also found that this compound is stable under other conditions, which it could encounter in cancer cells: pH 7.4 (cytoplasm), pH 5 (lysosome), and in the presence of H_2O_2 (ER) (Figure S11 and Table S3, Supporting Information). The high stability of the FeC is also retained in cells. In particular, we analyzed the extract of A2780 cells incubated with this compound (3 μM) for 1 and 24 h by using LC−MS (Figures S12−S14, Supporting Information). We detected only the parent compound after 1 h of incubation, whereas at the longer incubation time (24 h), we additionally detected metabolite **2a** (educt of **2** with GSH), which was formed with 10% yield. As discussed below, the biological effects, including the induction of the ER stress, occur already after 10 min of the incubation of **2** with cells. Therefore, the metabolite **2a** that formed much later is not expected to play a critical role in the activity of **2**. These data confirm that **2** acts via the different mechanism than the previously reported FeC_Cl_6.[26]

Uptake Mechanism, Intracellular Distribution, and Effects of FeC 2 on Intracellular Organelles. For the uptake studies, we selected 9 μM FeC's as the highest drug concentration not causing significant cell death at short incubation times (<8 h). In contrast to FeC **1**, the uptake of FeC **2** by BL-2 and A2780 cells is substantial at 37 °C (Figure 2A). That explains why **2** is a more potent anticancer agent than **1** (Table 1 and Figures S8 and S9, Supporting Information). The uptake of **2** is strongly inhibited at 5 °C (Student's *t*-test, $p < 0.01$, Figures 2A, S15, and S16, Supporting Information). The latter data indicate that the cellular transport of the FeC requires energy and, therefore, occurs via the active mechanism or mechanisms. We identified these to be clathrin- and caveolin-mediated endocytosis since chlorpromazine (CPZ) and genistein (GNS), which are inhibitors of these biochemical processes, suppress the uptake of **2** significantly ($p < 0.01$, Figures 2B and S18, Supporting Information). A mixture of CPZ and GNS affects the uptake of FeC **2** even more strongly than the individual inhibitors, indicating additive clathrin- and caveolin-mediated endocytosis (Figure S19, Supporting Information). In contrast, the inhibitor of organic anion transporters (OATs) bromsulfthalein (BSP) does not suppress the uptake, indicating that OATs are not involved in the transport of **2** (Figure 2B).

To evaluate the intracellular distribution of FeC **2**, we prepared its analogue containing a terminal alkyne moiety—FeC **5**, whose synthesis was described elsewhere.[28] Incubation of A2780 cells with FeC **5** (9 μM) for 0.5, 2, and 4 h followed by their fixation, treatment with either Alexa Fluor 488 azide or Alexa Fluor 594 azide under the conditions of Cu^+-catalyzed alkyne−azide cycloaddition "click" reaction, washing, and monitoring the signal of the Alexa Fluor dyes allowed visualization of the transport of the FeC (Figure 2C−E). We found that the fluorescence signal observed in A2780 cells treated with FeC **5** can be suppressed by the coincubation of **5** with the unlabeled **2**, indicating that both **5** and **2** bind to the same intracellular target or targets (Figure S20, Supporting Information). After incubation for 30 min, the FeC is located in the cellular periphery, which can be the cellular membrane and/or the FeC bound to the components of the active transport associated with the membrane (Figures 2C and S21, Supporting Information). At the longer incubation time (2 h), the FeC is located in the proximity of the nucleus that can be either ER or Golgi or both (Figures 2D and S21, Supporting Information). Attempts to conduct the colocalization experiments of these in situ formed dye conjugates with known ER- and lysosome (LY)-staining probes were not successful since the stringent washing used in such experiments affected the intracellular distribution of the conjugates. At the longest incubation time (4 h), the FeC is distributed evenly within the cell. For example, its signal is partially colocalized with the nuclear stain (Pearson's coefficient 0.55, Figures 2E and S21, Supporting Information).

Within cells, UPs are formed, processed, and eventually accumulated mostly in the ER and LYs. Correspondingly, if FeC **2** induces the accumulation of UPs (Figure 1B), one of these organelles or both of them might be stressed. We observed that after only 10 min of incubation with FeC **2**, the fluorescence of A2780 cells, stained with the ER-specific dye ER-tracker Green for an additional 20 min, is significantly reduced ($p < 0.01$), indicating that the ER is affected. The effect is saturated after 30 min of incubation (Figure 2F). In contrast, FeC **2** (up to 24 h incubation) does not change the fluorescence of the cells labeled with LY-specific dye acridine orange (Figures S22 and S23, Supporting Information) that

https://doi.org/10.1021/jacs.3c08827
J. Am. Chem. Soc. XXXX, XXX, XXX−XXX

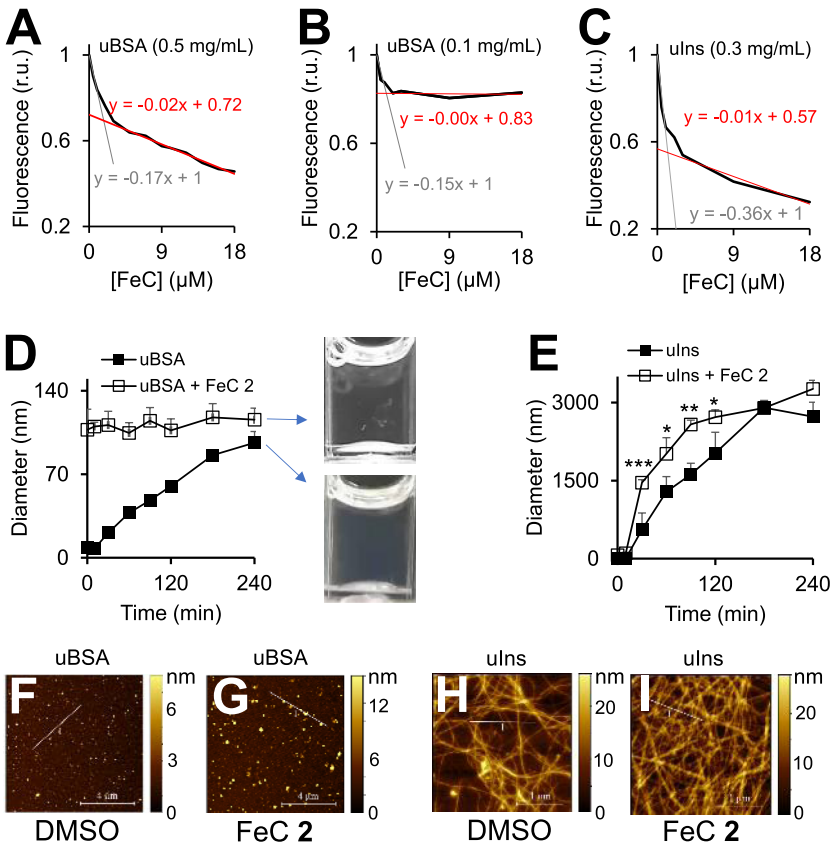

Figure 3. (A–C) Dependence of the fluorescence of associates of UPs (unfolded bovine serum albumin: uBSA or unfolded insulin: uIns) with thioflavin T (ThT, 10 μM, λ_{ex} = 440 nm; λ_{em} = 480 ± 10 nm) from the concentration of FeC **2**. Other conditions: incubation time, 100 min; temperature, 45 °C; DTT (1 mM for uBSA and 20 mM for uIns); and DMSO (1% (v/v)). (D) Kinetics of uBSA (0.5 mg/mL) aggregation in the presence of DTT (1 mM) at 22 °C were monitored by DLS. [FeC **2**] = 9 μM. The measurement at time point 0 min was performed before DTT addition. The size of the main peak was plotted vs the incubation period. Photos of cuvettes with uBSA and uBSA/FeC **2** samples after 240 min incubation are included. (E) Kinetics of uIns (0.3 mg/mL) aggregation in the presence of DTT (20 mM). Other conditions are as described in (D). AFM images of uBSA in the absence (F) and presence (G) of FeC **2**. AFM images of uIns in the absence (H) and presence (I) of FeC **2**. Height profiles along traces labeled with "l" are given in Figure S33, Supporting Information.

excludes LYs as the primary target of the FeC. Interestingly, treatment of the cells loaded with the Mit-specific dye rhodamine 123 (R123) with FeC **2** for 4 and 24 h also leads to the strong decrease of the R123 fluorescence, indicating that the FeC affects the Mit (Figures S22 and S23, Supporting Information). The latter effect is secondary to that on the ER since it appears at a substantially longer incubation time. In particular, the effect on the ER is saturated after 30 min incubation, whereas that on Mit is not saturated even after 4 h incubation (Figure S24, Supporting Information). By using JC-1, a dye sensitive to Mit membrane potential (MMP), we found that the FeC induces the decrease of MMP (Figures S25 and S26, Supporting Information).

Next, we determined whether the FeC is physically accumulated in particular organelles or whether the observed effects are indirect. These experiments required large cell numbers (5×10^7 cells) due to the technical limitations of the analytical method (AES) applied for monitoring Fe and B derived from the FeC in organelles (Supporting Information). We used BL-2 rather than A2780 cells since the former cells can be easily obtained in large quantities. We analyzed the content of ER, Mit, and LYs from the cells, which were preincubated with FeC **2** (9 μM) for 1 h, and found that only ER and Mit, but not LY fractions contain FeC **2** (Figures S27 and S28, Supporting Information). These data indicate that FeC is directly accumulated in the ER and Mit.

By using TEM (Figure 2G,H; more detailed images are provided in Figure S29, Supporting Information), we visualized morphological changes of the intracellular organelles in response to the FeC treatment. We found that the short (10 min) treatment of A2780 cells causes changes of morphology of Mit including the alteration of the cristae membrane and intracrystal space from typical parallel orientation (Figures 2G and S29A, Supporting Information) to less ordered intra-Mit structures (Figure S29C, Supporting Information). Furthermore, the FeC-treated cells contain ER's of irregular width and those exhibiting interruptions (Figure S29D, Supporting Information). These effects are strengthened under the prolonged treatment (4 h). For example, under the latter conditions, the cristae membrane is practically fully destroyed (Figures 2H and S29E, Supporting Information) and a number of swollen ER's are present (Figure S29F, Supporting Information).

Thus, according to the data described in this section, we could identify the ER as a primary target and Mit as a secondary target of FeC **2**.

Mechanism of Anticancer Activity of FeC 2. *Studies in Cell-Free Settings.* We considered two possible modes of action of FeC **2**, which could cause an effect on the ER, leading

https://doi.org/10.1021/jacs.3c08827
J. Am. Chem. Soc. XXXX, XXX, XXX−XXX

to the anticancer activity. First, this FeC can first bind UPs, inhibiting their maturation or inducing aggregation, thereby causing the ER stress. This possibility is based on the fact that the previously described analogues of **2**, clathrochelates Vz375,[24] and **1**[25] are binders of UPs in cell-free settings. Second, since FeC **2** is a complex of Fe^{2+}, it can potentially induce the generation of highly toxic species $O_2^{\bullet-}$ and HO• by donating an electron from the metal ion to the less toxic species O_2 and H_2O_2, thereby inducing oxidative stress in the ER and disturbing its function. It has been previously reported that ROS inducers can cause the ER stress, leading to cancer cell death.[10,11] In this section, the experiments will be described, which allowed us to confirm one of these possibilities.

To evaluate whether FeC **2** binds to UPs, we first selected unfolded bovine serum albumin (further uBSA) as a representative protein. uBSA was obtained by incubation of BSA with a dithiothreitol (DTT, 1 mM) at 45 °C. We confirmed formation of uBSA under these conditions by using thioflavin T probe (ThT, 10 μM), whose fluorescence is increased in the presence of unfolded and aggregated proteins[31] (Figure S30, Supporting Information). The increase of the fluorescence of the ThT/uBSA solutions (F100) is >90% complete after 100 min incubation. In further studies, we used normalized values of F100, which were obtained by dividing the fluorescence in the presence of FeC **2** at the concentration from 3 to 18 μM by the fluorescence in its absence (Figure 3A,B). F100 is strongly quenched by FeC in a dose-dependent fashion. Since in the absence of uBSA the FeC does not affect the fluorescence of ThT (Figure S31A, Supporting Information), the latter data indicate that the FeC binds to uBSA. The quenching curve obtained at the higher concentration of uBSA (0.5 mg/mL) is represented by two linear regions: the first one is steeper (F100 = −0.17 × [FeC **2**] + 1, black trendline), while the second one is more flat (F100 = −0.02 × [FeC **2**] + 0.72, red trendline) (Figure 3A). At a lower uBSA concentration (0.1 mg/mL), the latter region is absent. These data might indicate that the first region corresponds to binding of the FeC to uBSA and the second region to binding of the FeC to aggregated uBSA, whose formation is expected to be strongly concentration dependent. Interestingly, the same trend is observed in the quenching experiment, where uBSA was replaced with unfolded insulin (uIns, Figure 3C).

Due to limitations in solubility of FeC **2**, saturation of the quenching curves could not be reached (Figure 3A−C). Furthermore, binding of FeC **2** to products obtained after protein unfolding, followed by protein aggregation, is a complex process that makes it difficult to suggest a suitable model for fitting the experimental data. Due to these reasons, estimation of the binding constant of the FeC with the UPs was not possible based on the data shown in Figure 3A−C. In an attempt to address this issue, we applied isothermal titration calorimetry. We selected uIns rather than uBSA as a model protein due to its better water solubility. According to the baseline-corrected and blank-subtracted data, uIns binds FeC **2** in an exothermic process (Figure S32, Supporting Information). Unfortunately, the heat differences observed as well as the *c*-value were too small for the reliable determination of thermodynamic parameters of the uIns/FeC **2** interaction (Supporting Information). Reasons for that are limitations in the solubility of the reactants and heat compensation caused by the endothermic process of uIns dilution upon titration.

To study aggregation of the UPs in the presence of FeC **2**, we used DLS. We observed that the aggregates with a size of 110 ± 4 nm are formed immediately after mixing BSA (0.5 mg/mL) and FeC **2** (9 μM). Larger aggregates are not detected by DLS. However, they are also generated and, due to the low solubility in water, precipitated in the form of flakes (Figure 3D). In contrast, the uBSA aggregates grow substantially slowly ($t_{1/2}$ ∼ 120 min) in the absence of the FeC, and precipitation is not observed (Figure 3D). Aggregates of uIns are more soluble and do not precipitate. Therefore, steady growth of these species up to 3 μm in the presence of FeC **2** is observed within 240 min. In contrast, the growth rate of uIns is slower in the absence of FeC **2**. The latter data are confirmed by atomic force microscopy (AFM). In particular, uBSA forms <10 nm (in height) nanoparticles, whereas in the presence of FeC **2**, the size of the nanoparticles is increased up to 60 nm (Figures 3F,G and S33, Supporting Information). uIns form fibrils rather than nanoparticles. We observed that in the presence of FeC **2**, more fibrils were formed (Figure 3H,I). Moreover, the thickness of the fibrils is larger in the presence of FeC **2** than in the absence of FeC **2** (Figure S33, Supporting Information).

We observed that FeC **2** also binds the native proteins BSA and insulin. It is reflected in FeC **2**-induced quenching of the native protein fluorescence (Figure S34A, Supporting Information). The binding induces quick (<10 min) formation of aggregates of <110 nm diameter for both BSA and insulin (Figure S34B, Supporting Information). However, the amount of these aggregates seems to be small since they are not detected by AFM. Furthermore, in contrast to uBSA and uIns, no larger aggregates/precipitates are formed from native proteins and FeC **2** as evidenced by monitoring of light scattering of the corresponding suspensions (Figure S35, Supporting Information). This reaction will occur in normal cells lacking large amounts of UPs and can lead to undesired toxicity. Since only minute amounts of the aggregates will be formed, the negative impact is expected to be limited.

Next, we investigated whether FeC **2** can induce generation of highly reactive $O2^{\bullet-}$ and HO• from less toxic O_2 and H_2O_2 in cell-free settings under the conditions resembling the intracellular medium: aqueous buffer, pH 7.4, GSH 5 mM. In this experiment, we used a nonfluorescent probe 2′,7′-dichlorodihydrofluorescein (DCFH), which is oxidized to fluorescent 2′,7′-dichlorofluorescein (DCF) in the presence of $O2^{\bullet-}$ and HO•, but not O_2 and H_2O_2 (Figure S36, Supporting Information). We observed that FeC **2** does not accelerate the oxidation of DCFH at all. The reason for this behavior is its high redox potential of >1 V versus Ag/AgCl reference electrode as determined by cyclic voltamperometry (CV, Figure S37, Supporting Information).

Cellular Assays. We investigated whether FeC **2** binds to unfolded/aggregated proteins in living A2780 cells. The latter proteins were stained by ThT as described by Beriault and Werstuck.[31b] Additionally, the cells were loaded with LysoTracker Deep Red to stain lysosomes. The latter signal is not affected by FeC **2** (Figures S22 and S23, Supporting Information); therefore, it was used as a reference. We observed that the A2780 cells labeled in this way feature nonoverlapping green (ThT bound to unfolded/aggregated proteins) and red (lysosomes) signals. The treatment with FeC **2** (9 μM) leads to strong quenching of the green signal (Figure 4A,B, controls are provided in Figure S38, Supporting Information). By using flow cytometry, we confirmed that

https://doi.org/10.1021/jacs.3c08827
J. Am. Chem. Soc. XXXX, XXX, XXX−XXX

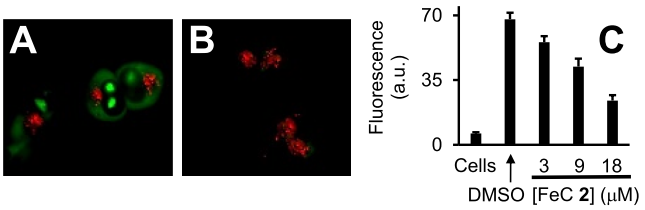

Figure 4. A2780 cells loaded with ThT (5 μM) and LysoTracker Deep Red (100 nM, reference) and treated either with carrier (DMSO, 1%, v/v) (A) or FeC **2** (9 μM) (B). Fluorescence images shown in A and B are both combinations of the green channel output (λ_{ex} = 470 ± 40 nm and λ_{em} = 525 ± 50 nm (monitoring ThT)) and red channel output (λ_{ex} = 640 ± 30 nm and λ_{em} = 690 ± 50 nm (monitoring LysoTracker Deep Red)). (C) Monitoring fluorescence of ThT-loaded A2780 cells (λ_{ex} = 405 nm and λ_{em} = 450 ± 45 nm) treated with either carrier ("DMSO") or FeC **2** (3–18 μM). Data for nonloaded cells ("cells") are shown for comparison. Error bars indicate the standard deviation. An unpaired Student's *t*-test was performed for statistical analysis. FeC **2** induces quenching of ThT-loaded cells: for 3 μM FeC **2**: $p < 0.05$; for 9 and 18 μM FeC **2**: $p < 0.001$.

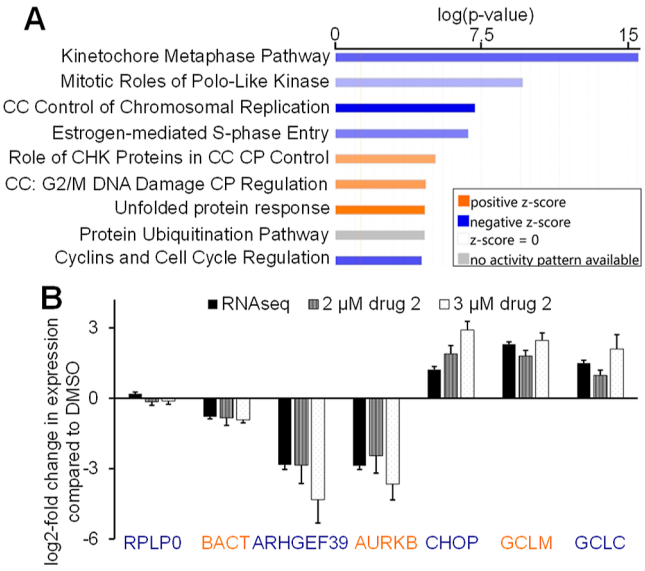

Figure 5. Impact of FeC **2** (2 μM, 1% DMSO, 24 h) on the transcriptome of A2780 cancer cells. (A) Most significantly altered canonical pathways. CC and CP are abbreviations for cell cycle and checkpoint, respectively. (B) Validation of the RNAseq experiment by determination of relative gene expression of the selected genes in the presence of 2 μM or 3 μM FeC **2** by using PCR. The data were normalized to GAPDH mRNA levels (N = 3, error bars indicate standard deviations).

this effect is dose dependent in the concentration range of 3–18 μM of FeC **2** (Figure 4C). These data indicate that FeC **2** binds to unfolded/aggregated proteins in living A2780 cells at the selected experimental conditions.

To get an overview of the signaling pathways that are affected by FeC **2**, we evaluated its effects on gene expression in A2780 cells by using next-generation sequencing (RNA-Seq). We determined the ratios of amounts of RNAs derived from known genes in the untreated and treated groups (FeC **2**: 2 μM, 24 h incubation) and defined these parameters as FoldChange. We selected the genes fulfilling the condition of $\log_2$ FoldChange < −2 and >2 for further analysis (Figure S40, Supporting Information). Based on the obtained data set and by using Ingenuity Pathway Analysis (IPA), we identified nine top scored canonical pathways induced or suppressed by the FeC (IPA, Figure 5A).

In agreement with the previous experiments (Figure 2), two of these pathways are related to ER stress: UPR and protein ubiquitination pathways. The detailed effect of FeC **2** on the expression of genes belonging to these pathways is outlined in Figure S41A,B, Supporting Information. We validated the latter result in the following four groups of independent experiments. First, we confirmed the overexpression of C/EBP homologous protein (CHOP) mRNA in A2780 cells treated with FeC **2** using PCR (Figure 5B). CHOP(GADD153) is a transcription factor known to be activated under the ER stress.[2] Second, we observed that the level of ubiquitinated proteins increased in the treated A2780 cells (Figure 6A). The latter data indicated that the treatment with the FeC leads to the amplification of UPs prepared for removal via the ER-associated protein degradation (ERAD) system including the ubiquitin–proteasome pathway.[2] Third, we detected the formation of the elevated amount of spliced XBP1 (sXBP1)-mRNA transcript 10 min after the treatment of A2780 cells with FeC **2** (Figures 6B and S43, Supporting Information). These data indicate the activation of eukaryotic translation initiation factor 2 alpha kinase 3 (PERK) and inositol requiring enzyme 1 (IRE1) arms of UPR.[2a] In contrast, the activating transcription factor 6 (ATF6) arm seems to be activated to a lesser extent (Figure S41 and the summary afterward, Supporting Information). Fourth, we observed the upregulation of the antioxidant intracellular system controlled by nuclear factor erythroid-2 related factor 2 (NRF2). This was evident from the enhanced expression of NRF2 target genes glutamate–cysteine ligase regulatory protein (GCLM) and glutamate–cysteine ligase catalytic subunit (GCLC)[32] (Figure 5B).

Further, we found that in A2780 cells treated with FeC **2**, the levels of mitochondrial ROS (mROS) (Figures 6C and, S44, Supporting Information) and NO are increased in dose- and incubation time-dependent ways (Figure S46, Supporting Information). mROS ($O_2^{\bullet-}$) and NO can combine in cells with the formation of a highly reactive peroxynitrite anion ($ONOO^-$).[33] The latter chemical species induce strong oxidative stress in the cancer cells that should be the cause of the activation of the NRF2 system. Potentially, ROS can be produced either indirectly as a consequence of the ER stress[34] or directly by donation of an electron from FeC **2** to O_2 and H_2O_2. We excluded the latter possibility based on two experiments. First, we confirmed that the redox potential of FeC **2** is too high to act as a catalyst in ROS generation (Figures S36 and S37, Supporting Information). Second, we observed that FeC **2** does not induce production of total ROS (tROS) in A2780 cells, which is detected using 5-(and-6)-chloromethyl-2′,7′-dichlorodihydrofluorescein diacetate (CMDCFH-DA) as a probe (Figure S47, Supporting Information). In contrast, known iron-containing compounds capable of the direct ROS generation in cell-free settings and in cells, e.g., aminoferrocene-based prodrugs, usually increase the level of intracellular tROS.[11,35,36]

Next, we studied the effects of FeC **2** in representative normal cells SBLF9. These cells were selected since they contain the lower level of intracellular unfolded/aggregated proteins compared to cancer A2780 cells (Figure S43, Supporting Information). According to the suggested mode of action (Figure 1B), we expected that FeC **2** would induce

https://doi.org/10.1021/jacs.3c08827
J. Am. Chem. Soc. XXXX, XXX, XXX−XXX

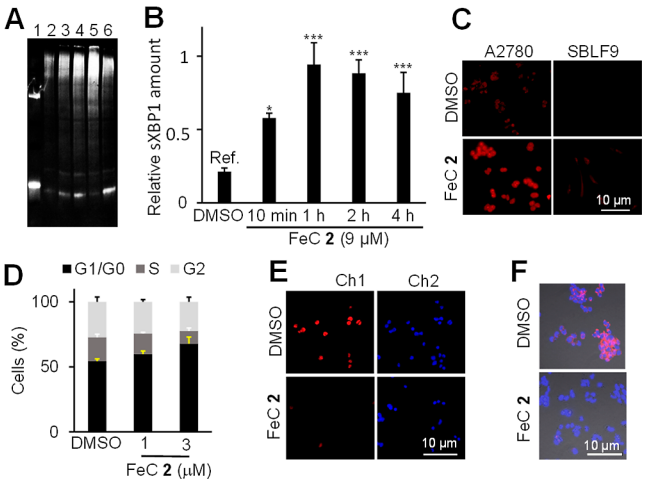

Figure 6. (A) Protein ubiquitination in A2780 cells upon treatment with DMSO (2); FeC **2** (9 μM, 30 min incubation) (3); as (2) except for 4 h incubation (4); upon treatment with bortezomib (500 nM); 4 h incubation (5); control **1** (30 μM); and 4 h incubation (6) as detected by western blotting using antiubiquitin (E412J) rabbit mAB and antirabbit AlexaFluor488 secondary antibodies. Fluorescence imaging was performed with an iBright FL1000 λ_{ex} = 455−485 nm and λ_{em} = 510−555. (B) Kinetics of ER stress induction in A2780 cells after incubation for 10 min−4 h with FeC **2** (9 μM) and subsequent determination of relative sXBP1 concentrations by qPCR using RPLP0 as a housekeeping gene. (C) Fluorescence of MitoSOX-loaded A2780 and SBLF9 cells incubated either with DMSO (1%, v/v) or FeC **2** (9 μM, incubation time 2 h) determined by fluorescence microscopy. (D) Effects of FeC **2** on the cell cycle of A2780 cells: incubation time 24 h. (E) Effects of FeC **2** (9 μM, incubation time 4 h) on the *de novo* synthesis of DNA as determined by using deoxyethynyluridine treatment (2 mM, 2 h) and subsequent reaction of all DNA-incorporated alkyne groups with an Alexa Fluor 594 azide. Red channel Ch1: λ_{ex} = 545 ± 25 nm and λ_{em} = 605 ± 70 nm. Blue channel, Ch2: λ_{ex} = 365 nm and λ_{em} = 445 ± 50 nm. (F) A2780 cells were treated with either DMSO (1%, v/v) or FeC **2** (3 μM, 1% DMSO) for 24 h followed by fixation and staining with phalloidin-Atto655 (red signal: λ_{ex} = 640 ± 30 nm and λ_{em} = 690 ± 50 nm) and Hoechst 33342 (blue signal: λ_{ex} = 365 nm and λ_{em} = 445 ± 50 nm). An unpaired Student's *t*-test was performed for statistical analysis (*: $p < 0.05$; **: $p < 0.01$; and ***: $p < 0.001$).

less or no effect in SBLF9 cells. In agreement with this expectation, we observed that FeC **2** (9 μM) does not increase intracellular levels of spliced XBP1, mROS, and NO at 1 h incubation time. In contrast, under the same conditions, spliced XBP1, mROS, and NO are significantly upregulated in cancer A2780 cells (Figures 6C, S43C, S45, and S46B, Supporting Information). Thus, these data support the concept of BUPs introduced above (Figure 1B).

A known effect of the ER stress is the growth arrest in the G1 phase of the cell cycle[37] as well as the inhibition of expression of many genes related to these process.[38] In agreement with this expectation, we observed that seven of nine top-scored pathways affected by the FeC in A2780 cells, as identified by RNA-Seq, are related to the cell cycle and DNA and RNA synthesis (Figure 5A). We validated this result by the following two experiments. First, we observed that the cell cycle arrest in the G1 phase is induced upon treatment of A2780 cells with FeC **2** (Figure 6D). Second, we found that the FeC inhibits the *de novo* synthesis of DNA (Figure 6E, Supporting Information) and RNA (Figure S49, Supporting Information) in A2780 cells. Furthermore, Rho Guanine Nucleotide Exchange Factor 39 (ARHGEF39) is downregulated by FeC **2** according to RNA-Seq and PCR (Figure 5). ARHGEF39 protein is known to promote cell proliferation.[39] All these data (G1 phase cell cycle arrest, inhibition of the DNA and RNA synthesis, as well as the effect on ARHGEF39) contribute to antiproliferative properties of the FeC.

Surprisingly, FeC **2** treatment of A2780 cells leads to downregulation of expression of β-actin (ACTB) as confirmed by RNA-Seq and validated by PCR (Figure 5B). We also observed that it is accompanied by a decrease of the level of intracellular filamentous β-actin protein (Figure 6F). Since β-actin is upregulated in the majority of cancer cells and is associated with invasiveness and metastasis of cancer,[40] these data could indicate that the FeC has a potential as an antimetastatic drug. We confirmed that it is indeed the case in two experiments. First, we observed that FeC **2** (3 μM) substantially slows down the migration of human lung cancer SK-MES-1 cells in wound healing assay (Figure S50, Supporting Information). Second, we found that the FeC exhibits antimetastatic activities in vivo, as described in the next section.

Together with the ER stress and the associated oxidative stress, the effects of the FeC on cell cycle, DNA/RNA synthesis, and cell proliferation induce cancer cell death (Table 1). We determined that the FeC **2** mediated death of A2780 and BL-2 cells occurs via apoptosis and necrosis (Figures S51−S57, Supporting Information). The cells can be rescued by PERK-inhibitor I and scavengers of ROS (N-acetylcysteine, NecroX5 methanesulfonate, and ascorbic acid). In contrast, the Ca^{2+} scavenger BAPTA and the NOX2 inhibitor DPI exhibit no effect. These data indicate that the upregulated UPR and ROS, but not Ca^{2+} and NOX2, play important roles in the anticancer activity of FeC **2**. Despite ROS being involved, according to our data discussed above, the upstream factor of the activity of FeC **2** is the amplification of UPs caused by the ER stress and eventually the cell death in cancer cells.

Next, we benchmarked FeC **2** with respect to the known inducers of ER stress. In particular, effects of FeC **2** (9 μM), an inhibitor of 26S proteasome bortezomib (0.5 μM), and an inhibitor of sarcoplasmic/ER calcium ATPase (SERCA) thapsigargin (0.5 μM) were compared with each other in four selected assays. Nontoxic concentrations of the inhibitors were selected. A summary of inhibitor rankings corresponding to their performance in these assays (first, second, and third place) is provided in Table 2.

In particular, we found that FeC **2** strongly enhances mROS in A2780 cells (2.5 fold, $p < 0.001$), whereas bortezomib is inactive ($p < 0.05$), and thapsigargin even slightly reduces the

Table 2. Efficacy of Drugs Inducing ER Stress (first to third Places)[a] in Four Selected Assays

	ranking of drugs in the following assays			
drug[b]	mROS level	ER staining	CHOP expression	XBP1 splicing
FeC **2**	1st	1st	3rd	2nd
thapsigargin	2nd	2nd	1st	1st
bortezomib	2nd	3rd	2nd	3rd

[a]1st place: a drug with the strongest effect. 3rd place: a drug with the weakest effect. [b][FeC **2**] = 9 μM, [thapsigargin] = [bortezomib] = 0.5 μM.

https://doi.org/10.1021/jacs.3c08827
J. Am. Chem. Soc. XXXX, XXX, XXX−XXX

amount of mROS ($p < 0.05$) (Figure S58A, Supporting Information). Similarly, FeC **2** has the strongest effect on ER staining among this group of drugs (Figure S58B, Supporting Information). In contrast, thapsigargin is the most potent enhancer of CHOP expression ($p < 0.001$), followed by bortezomib ($p < 0.001$), whereas FeC **2** exhibits the weakest effect ($p < 0.01$) (Figure S58C, Supporting Information). Finally, thapsigargin is the strongest inducer of the XBP1 splicing ($p > 0.001$), followed by FeC **2** ($p < 0.05$), whereas bortezomib is inactive under the selected conditions (Figure S58D, Supporting Information). These data indicate that FeC **2** exhibits the unique action profile as reflected in Table 2, which indicates that its mechanism of action is different from that of the known ER stress inducers tested here.

Antitumor and Antimetastatic Activity of FeC 2 and Its Toxicity toward Blood Cells and Bone Marrow In Vivo. Encouraged by excellent anticancer activity (Table 1) and cancer cell specificity (Figures 6C, S43C, S45, and S46B, Supporting Information) observed in vitro, we studied whether FeC **2** retains these favorable properties in vivo. First, we found that the lethal dose (LD) of FeC **2**, injected intraperitoneally (i.p.) in C57/BL6 mice, is between 147 and 246 mg/kg (Table S16, Supporting Information). The lethality of the FeC at the high dose can be caused by its activation by low amounts of unfolded/aggregated proteins or by its direct effect on proteins (Figure S34, Supporting Information).

Next, we investigated the antitumor effect of FeC in Nemeth-Kellner lymphoma (NK/Ly), grown as solid tumors of myeloid sarcoma. This is a standard model for testing new chemotherapeutics in our laboratories.[33,39] Untreated animals had a half-life of 32 days. For this therapy experiment, we selected the dose of 12 mg/kg for a single injection. The compound was injected i.p. every second day for 10 times. The treatment did not cause any adverse effects. For example, the animals did not lose weight over 93 days of the experiment (Figure S59, Supporting Information). Moreover, the internal organs of animals dissected at the end of the experiment did not show any abnormalities (Figure S62, Supporting Information). The resulting Kaplan−Meier (survival) plot is shown in Figure 7A.

The mean survival time is statistically significantly increased in the group treated with the FeC as compared to the group, which received only the carrier: from 32 to 75 days ($p < 0.0001$). On day 93, three survived mice in the treated group (27% from the initial number of the animals: 11) were killed and dissected. We detected no signs of tumors, indicating that these animals were completely cured (Figure S62, Supporting Information). This is an exciting result, which we have previously never observed for other Fe-containing drugs.[35,41] Due to the excellent performance in the standard tumor model, we have also investigated its effects in the second, more challenging NK/Ly model, in which the cancer cells grow in the abdomen as ascites. This cancer is very aggressive, and untreated animals have a half-life of only 18 days. We were pleased to observe the moderate activity of FeC **2**. In particular, treatment with the FeC prolonged the life span of mice from 18 to 22 days ($p < 0.05$) (Figure 7B). On day 13 of this experiment, we collected ascites from the mice (0.3 mL, lymphoma tumor cells), treated them with TBMS-306[42] (20 nM), a probe sensitive to MMP, and detected their fluorescence by fluorescence microscopy. We observed a strong signal in the control group and practically no signal in the FeC **2**-treated group (Figure 7C). In a similar experiment,

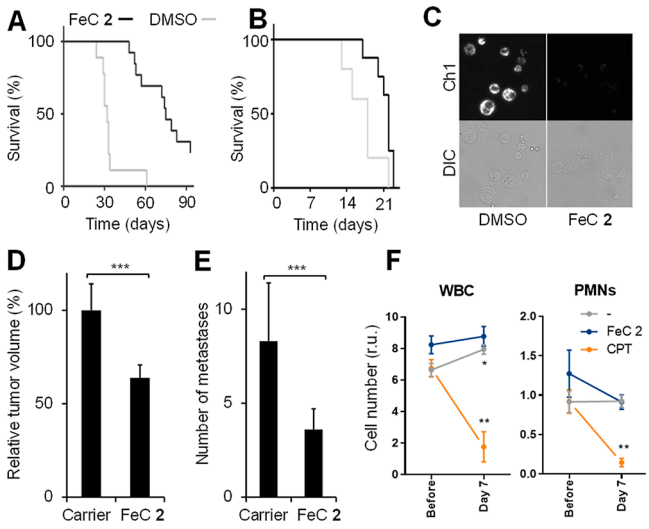

Figure 7. (A) Survival of animals with NK/Ly myeloid sarcoma (A) and lymphoma (B) in the control (DMSO) and FeC **2**-treated groups. Experimental details are provided in the Supporting Information. (C) Fluorescent microscopy of NK/Ly lymphoma cells grown in the abdominal cavity of mice isolated after 13 days of treatment either with the carrier (DMSO) or FeC **2** and stained with TBMS-306 (20 nM, 10 min) (λ_{ex} = 630 nm and λ_{em} = 720 nm, Ch1). DIC = brightfield images. (D,E) Antitumor (C) and antimetastatic (D) effects of FeC **2** in a murine Lewis lung carcinoma LLC1 model were observed on 22 day of the experiment. An unpaired Student's *t*-test was performed for statistical analysis: *—$p < 0.05$; **—$p < 0.01$; and ns—$p > 0.05$. (F) Monitoring of the number of white blood cells (WBC) and neutrophils (PMNs) in blood. The analysis was conducted on day 7. Paired *t*-test was conducted between days 0 and 7. *: $p < 0.05$; **: $p < 0.01$; and ***: $p < 0.001$. The data for other blood and BM cells are provided in Figure S53, Supporting Information.

in which TBMS-306 was replaced with an MMP-independent Mit-probe TBMS-52[43] (20 nM), no difference between both groups was observed (Figure S60, Supporting Information). These data indicate that in vivo, the FeC acts via the reduction of MMP, whereas the shape and size of Mit are not affected. Similar effects of the FeC on the MMP of A2780 cells were also observed in vitro (Figures S25 and S26, Supporting Information).

On day 23 of the experiment with the myeloid sarcoma model, one mouse from the control, and one from the treated groups were killed, and histology of tumor slices was conducted. We observed an increase in the number of cancer cells with fragmented nuclei in the treated group, indicating that the FeC promotes cancer cell apoptosis in vivo (Figure S61, Supporting Information). As described above, FeC also induces apoptosis of A2780 and BL-2 cells in vitro (Figures S51−S57, Supporting Information). Thus, at least two effects of FeC including the decrease of MMP and cell death via apoptosis are observed both in vivo and in vitro. These data may indicate that the modes of action of FeC in vitro and in vivo are similar. Importantly, we observed that also in this more challenging NK/Ly model, treatment with FeC **2** does not induce the loss of animal weight, indicating its good tolerability (Figure S59, Supporting Information).

The FeC affects the expression of β-actin and inhibits cell migration in vitro (Figure S50, Supporting Information). These preliminary studies justified the evaluation of anti-metastatic properties of FeC in vivo. We selected murine Lewis

https://doi.org/10.1021/jacs.3c08827
J. Am. Chem. Soc. XXXX, XXX, XXX−XXX

lung carcinoma LLC1 model, in which LLC1 cells grow as a primary tumor and form numerous metastases in lungs. The treatment included the i.p. injection of the FeC (48 mg/kg) twice per week for 3 weeks. On the 22nd day, the tumor volume as well as the number and volume of metastases were evaluated (Figures 7D,E and S63, Supporting Information). We observed significant reduction of volume of the primary tumor ($p < 0.001$) and the number ($p < 0.001$) and volume ($p < 0.05$) of metastases in the treated group as compared to the control group.

Finally, we investigated the in vivo toxicity of the FeC toward a range of noncancerous cells at the therapeutically active dose of 12 mg/kg. They included white blood cells (WBC), red blood cells (RBC), platelets, polymorphonuclear neutrophils (PMNs), monocytes (MONO), and lymphocytes (LYM) from blood. We also studied the effect of the FeC on BM cellularity and on the following BM cells: CD45+ cells, PMNs, MONO, B and T cells, LineageNEG Sca-1+ c-Kit+ cells, and myeloid progenitors. As a positive control, we applied camptothecin (CPT), which exhibited strong toxicity toward the majority of these cells (Figures 7F and S64, Supporting Information). In contrast, no statistically significant toxicity of FeC was observed (Figures 7F and S64, Supporting Information) that is in agreement with good tolerability of this compound and its inability to generate mROS and NO and induce the ER stress (no sXBP1 upregulation) in representative normal SBLF9 cells as observed in vitro (Figures 6C, S43, S45, and S46B, Supporting Information).

CONCLUSIONS

Known Fe^{2+}-clathrochelates binding UPs (e.g., FeC **1**) are not cell membrane permeable and, therefore, do not exhibit anticancer activity. By the variation of their structure, we discovered FeC **2** containing a critical carboxylic acid moiety. Structurally, FeC resembles fullerene C_{60}. However, in contrast to the latter carbon allotrope, it is more water soluble. The FeC can be considered as an inorganic mimic of C_{60} suitable for medicinal applications. The FeC exhibits high to moderate anticancer activity toward a range of cancer cell lines derived from blood (HL-60, BL-2, Jurkat), ovary (A2780), and lungs (SK-MES1, LLC1). Furthermore, its activity is retained in vivo, as confirmed for two Nemeth-Kellner lymphoma models and an LLC1 lung cancer model. In cells, the FeC acts as a monomer rather than an aggregate. It is stable in cells at the shorter incubation time (1 h) but is partially (10%) metabolized to its educt with glutathione at the longer incubation time (24 h). The latter metabolite does not contribute to the anticancer activity since the initial cellular effects of the FeC, including the induction of the ER stress, appear very quickly at <10 min incubation time. The FeC is efficiently uptaken by cancer cells via the active mechanism mediated by clathrin and caveolin. In cells, it first induces the ER stress due to the accumulation of UPs as evidenced by the activation of the protein ubiquitination pathway, which is reflected in the upregulation of its genes and the increase of the amount of intracellular ubiquitinated proteins. The initial effect on the ER leads later on to the decrease of mitochondrial membrane potential, induction of oxidative stress including the formation of mitochondrial ROS, upregulation of NO as well as growth arrest in the G1 phase, and inhibition of DNA and RNA synthesis. All these factors cause cell apoptosis and partially necrosis. Importantly, in contrast to cancer cells, the FeC does not affect the ROS, NO, and sXBP1 levels in representative noncancerous SBLF9 cells, indicating its cancer cell specificity. We confirmed that at its active dose of 12 mg/kg, the FeC does not induce any toxic effects on a range of cells in blood (white and red blood cells, platelets, neutrophils, monocytes, and lymphocytes) and bone marrow (CD45+ cells, neutrophils, monocytes, B and T cells, lineageNEG Sca-1+ c-Kit+ cells, and myeloid progenitors). Finally, the FeC exhibits significant antimetastatic activity in the LLC1 lung cancer model. These data are in agreement with the FeC-mediated inhibition of β-actin expression and reduction of β-actin levels in cells observed in vitro.

In summary, FeC **2** is a metal-containing anticancer agent acting via a novel mechanism based on the intracellular UP amplification in the ER and exhibiting high cancer cell specificity and, correspondingly, low toxicity as confirmed in vitro and in vivo.

ASSOCIATED CONTENT

Supporting Information

The Supporting Information is available free of charge at https://pubs.acs.org/doi/10.1021/jacs.3c08827.

Synthesis protocols, analytics, experimental details, in vitro experiments not described in the main paper, and detailed in vivo data (PDF)

AUTHOR INFORMATION

Corresponding Author

Andriy Mokhir − *Department of Chemistry and Pharmacy, Organic Chemistry II, Friedrich-Alexander-University of Erlangen-Nürnberg (FAU), 91058 Erlangen, Germany;* orcid.org/0000-0002-9079-5569; Email: Andriy.Mokhir@fau.de

Authors

Insa Klemt − *Department of Chemistry and Pharmacy, Organic Chemistry II, Friedrich-Alexander-University of Erlangen-Nürnberg (FAU), 91058 Erlangen, Germany*

[‡‡]**Oleg Varzatskii** − *Princeton Biomolecular Research Laboratories, 01042 Kyiv, Ukraine; V.I. Vernadsky Institute of General and Inorganic Chemistry, NASU, 03142 Kyiv, Ukraine*

Roman Selin − *Department of Chemistry and Pharmacy, Organic Chemistry II, Friedrich-Alexander-University of Erlangen-Nürnberg (FAU), 91058 Erlangen, Germany*

Serhii Vakarov − *Princeton Biomolecular Research Laboratories, 01042 Kyiv, Ukraine; V.I. Vernadsky Institute of General and Inorganic Chemistry, NASU, 03142 Kyiv, Ukraine*

[‡‡]**Vladyslava Kovalska** − *Princeton Biomolecular Research Laboratories, 01042 Kyiv, Ukraine; Institute of Molecular Biology and Genetics, NASU, 03143 Kyiv, Ukraine*

Galyna Bila − *Department of Histology, Cytology and Embryology, Danylo Halytsky Lviv National Medical University, 79010 Lviv, Ukraine; Lectinotest R&D, 79024 Lviv, Ukraine*

Rostyslav Bilyy − *Department of Histology, Cytology and Embryology, Danylo Halytsky Lviv National Medical University, 79010 Lviv, Ukraine; Lectinotest R&D, 79024 Lviv, Ukraine;* orcid.org/0000-0002-2344-1349

Yan Voloshin − *Nesmeyanov Institute of Organoelement Compounds, RAS, 119334 Moscow, Russia;* orcid.org/0000-0003-2823-6560

https://doi.org/10.1021/jacs.3c08827
J. Am. Chem. Soc. XXXX, XXX, XXX−XXX

Itziar Cossío Cuartero − *Program of Cardiovascular Regeneration, Centro Nacional de Investigaciones Cardiovasculares Carlos III (CNIC), 28029 Madrid, Spain*
Andrés Hidalgo − *Program of Cardiovascular Regeneration, Centro Nacional de Investigaciones Cardiovasculares Carlos III (CNIC), 28029 Madrid, Spain*
Benjamin Frey − *Department of Radiation Oncology, Translational Radiobiology, Universitaetsklinikum Erlangen, Friedrich-Alexander-University of Erlangen-Nürnberg (FAU), 91054 Erlangen, Germany*
Ina Becker − *Department of Radiation Oncology, Translational Radiobiology, Universitaetsklinikum Erlangen, Friedrich-Alexander-University of Erlangen-Nürnberg (FAU), 91054 Erlangen, Germany*
Bernhard Friedrich − *Department of Otorhinolaryngology, Head and Neck Surgery, Section of Experimental Oncology and Nanomedicine (SEON), University Hospital, Friedrich-Alexander-University of Erlangen-Nürnberg (FAU), 91054 Erlangen, Germany*
Rainer Tietze − *Department of Otorhinolaryngology, Head and Neck Surgery, Section of Experimental Oncology and Nanomedicine (SEON), University Hospital, Friedrich-Alexander-University of Erlangen-Nürnberg (FAU), 91054 Erlangen, Germany;* orcid.org/0000-0001-9306-633X
Ralf P. Friedrich − *Department of Otorhinolaryngology, Head and Neck Surgery, Section of Experimental Oncology and Nanomedicine (SEON), University Hospital, Friedrich-Alexander-University of Erlangen-Nürnberg (FAU), 91054 Erlangen, Germany*
Christoph Alexiou − *Department of Otorhinolaryngology, Head and Neck Surgery, Section of Experimental Oncology and Nanomedicine (SEON), University Hospital, Friedrich-Alexander-University of Erlangen-Nürnberg (FAU), 91054 Erlangen, Germany*
Elena-Laura Ursu − *"Petru Poni" Institute of Macromolecular Chemistry, Romanian Academy, Centre of Advanced Research in Bionanoconjugates and Biopolymers, 700487 Iasi, Romania*
Alexandru Rotaru − *"Petru Poni" Institute of Macromolecular Chemistry, Romanian Academy, Centre of Advanced Research in Bionanoconjugates and Biopolymers, 700487 Iasi, Romania*
Iris Solymosi − *Department of Chemistry and Pharmacy, Organic Chemistry II, Friedrich-Alexander-University of Erlangen-Nürnberg (FAU), 91058 Erlangen, Germany*
M. Eugenia Pérez-Ojeda − *Department of Chemistry and Pharmacy, Organic Chemistry II, Friedrich-Alexander-University of Erlangen-Nürnberg (FAU), 91058 Erlangen, Germany*

Complete contact information is available at: https://pubs.acs.org/10.1021/jacs.3c08827

Funding

We thank European Commission (861878: NeutroCure; 778245: Clathroprobes; and 872331: NoBiasFluors), Schmauser-Stiftung; and Friedrich-Alexander-Universität Erlangen-Nürnberg for funding this study. IK acknowledges the support of Studienstiftung for a doctoral fellowship. RS acknowledges the support of Alexander von Humboldt-Stiftung for a postdoctoral fellowship. The CNIC is supported by the MCIN and the Pro CNIC Foundation and is a Severo Ochoa Center of Excellence (CEX2020-001041-S). We gratefully acknowledge the generous support by the Manfred Roth-Stiftung, Fürth (Germany), as well as by the Forschungsstiftung Medizin am Universitsätsklinikum Erlangen (Germany).

Notes

The authors declare no competing financial interest.
‡‡O. Varzatskii: date of death—20.12.2017; V Kovalska: date of death—03.12.2020.

■ ACKNOWLEDGMENTS

We thank Prof. Dr. Andreas Hirsch for allowing the extensive usage of the infrastructure of his chair Organic Chemistry II at FAU. Confocal microscopy was performed on a Zeiss Spinning Disc Axio Observer Z1, funded by Deutsche Forschungsgemeinschaft (DFG, German Research Foundation)—project 248122450. Tumor tissue imaging was done using infrastructure established under National Research Foundation of Ukraine grant 2020.02.0131.

■ ABBREVIATIONS

ACTB, β-actin; AES, atomic emission spectroscopy; AFM, atomic force microscopy; ARHGEF39, Rho Guanine Nucleotide Exchange Factor 39; BSA, bovine serum albumin; BUP, binders of Ups; BSP, bromsulfthalein; CHOP, C/EBP homologous protein; CMDCFH-DA, 5-(and-6-)-chloromethyl-2′,7′-dichlorodihydrofluorescein; CPT, camptothecin; CPZ, chloropromazine; CUC, coordinatively unsaturated complexes; CV, cyclic voltamperometry; DCFH, 2′,7′-dichlorodihydrofluorescein; DCF, 2′,7′-dichlorofluorescein; DLS, dynamic light scattering; DTT, dithiothreitol; ER, endoplasmic reticulum; ERAD, ER-associated protein degradation; FBS, fetal bovine serum; GCLC, glutamate−cysteine ligase catalytic subunit; GCLM, glutamate−cysteine ligase regulatory protein; Gln, glutathione; GNS, genistein; GSH, glutathione; LD, lethal dose; LY, lysosome; Mit, mitochondria; MMP, mitochondrial membrane potential; MONO, monocytes; mROS, mitochondrial ROS; NO, nitric oxide; NRF2, nuclear factor erythroid-2 related factor 2; PBS, phosphate buffered saline; PMN, neutrophils; RBC, red blood cells, R123, rhodamine 123; ROS, reactive oxygen species; sXBP1, spliced XBP1 mRNA; TEM, transmission electron microscopy; ThT, thioflavin T; tROS, total ROS; uINS, unfolded insulin; UP, unfolded proteins; UPR, unfolded protein response; WBS, white blood cells; WBC, white blood cells

■ REFERENCES

(1) (a) Hurley, L. H. DNA and its associated processes as targets for cancer therapy. *Nat. Rev. Cancer* **2002**, *2*, 188−200. (b) Palchaudhuri, R.; Hergenrother, P. J. DNA as a target for anticancer compounds: methods to determine the mode of binding and the mechanism of action. *Curr. Opin. Biotechnol.* **2007**, *18*, 497−503. (c) van den Boogaard, W. M. C.; Komninos, D. S. J.; Vermeij, W. P. Chemotherapy Side-Effects: Not All DNA Damage Is Equal. *Cancers* **2022**, *14*, 627.
(2) (a) Chen, X.; Cubillos-Ruiz, J. R. Endoplasmic reticulum stress signals in the tumour and its microenvironment. *Nat. Rev. Cancer* **2021**, *21*, 71−88. (b) King, A. P.; Wilson, J. J. Endoplasmic reticulum stress: an arising target for metal-based anticancer agents. *Soc. Rev.* **2020**, *49*, 8113−8136.
(3) Richardson, P. G.; Sonneveld, P.; Schuster, M. W.; Irwin, D.; Stadtmauer, E. A.; Facon, T.; Harousseau, J.-L.; Ben-Yehuda, D.; Lonial, S.; Goldschmidt, H.; Reece, D.; San-Miguel, J. F.; Bladé, J.; Boccadoro, M.; Cavenagh, J.; Dalton, W. S.; Boral, A. L.; Esseltine, D. L.; Porter, J. B.; Schenkein, D.; Anderson, K. C. Bortezomib or high-

dose dexamethasone for relapsed multiple myeloma. *N. Engl. J. Med.* **2005**, *352*, 2487−2498.
(4) (a) Usmani, S. Z.; Quach, H.; Mateos, M. V.; Landgren, O.; Leleu, X.; Siegel, D.; Weisel, K.; Gavriatopoulou, M.; Oriol, A.; Rabin, N.; Nooka, A.; Qi, M.; Beksac, M.; Jakubowiak, A.; Ding, B.; Zahlten-Kumeli, A.; Yusuf, A.; Dimopoulos, M. Carfilzomib, dexamethasone, and daratumumab versus carfilzomib and dexamethasone for patients with relapsed or refractory multiple myeloma (CANDOR): updated outcomes from a randomised, multicentre, open-label, phase 3 study. *Lancet Oncol.* **2022**, *23*, 65−76. (b) Dimopoulos, M. A.; Goldschmidt, H.; Niesvizky, R.; Joshua, D.; Chng, W. J.; Oriol, A.; Orlowski, R. Z.; Ludwig, H.; Facon, T.; Hajek, R.; Weisel, K.; Hungria, V.; Minuk, L.; Feng, S.; Zahlten-Kumeli, A.; Kimball, A. S.; Moreau, P. Carfilzomib or bortezomib in relapsed or refractory multiple myeloma (ENDEAVOR): an interim overall survival analysis of an open-label, randomised, phase 3 trial. *Lancet Oncol.* **2017**, *18*, 1327−1337.
(5) (a) Chen, X.; Yang, Q.; Xiao, L.; Tang, D.; Dou, Q. P.; Liu, J. Metal-based proteasomal deubiquitinase inhibitors as potential anticancer agents. *Met. Rev.* **2017**, *36*, 655−668. (b) Zhang, Z.; Wang, H.; Yan, M.; Wang, H.; Zhang, C. Novel copper complexes as potential proteasome inhibitors for cancer treatment. *Mol. Med. Rep.* **2017**, *15*, 3−11. (c) Karges, J.; Stokes, R. W.; Cohen, S. M. Metal complexes for therapeutic applications. *Trends Chem.* **2021**, *3* (7), 523−534. (d) Zhang, L.; Montesdeoca, N.; Karges, J.; Xiao, H. Immunogenic cell death inducing metal complexes for cancer therapy. *Angew. Chem., Int. Ed.* **2023**, *62*, No. e202300662.
(6) (a) Mandic, A.; Hansson, J.; Linder, S.; Shoshan, M. C. Cisplatin induces endoplasmic reticulum stress and nucleus-independent apoptotic signaling. *J. Biol. Chem.* **2003**, *278*, 9100−9106. (b) Johnstone, T. C.; Suntharalingam, K.; Lippard, S. J. The Next Generation of Platinum Drugs: Targeted Pt(II) Agents, Nanoparticle Delivery, and Pt(IV) Prodrugs. *Chem. Rev.* **2016**, *116*, 3436−3486.
(7) Fiskus, W.; Saba, N.; Shen, M.; Ghias, M.; Liu, J.; Gupta, S. D.; Chauhan, L.; Rao, R.; Gunewardena, S.; Schorno, K.; Austin, C. P.; Maddocks, K.; Byrd, J.; Melnick, A.; Huang, P.; Wiestner, A.; Bhalla, K. N. Auranofin induces lethal oxidative and endoplasmic reticulum stress and exerts potent preclinical activity against chronic lymphocytic leukemia. *Cancer Res.* **2014**, *74*, 2520−2532.
(8) Ramos, R.; Gilles, J. F.; Morichon, R.; Przybylski, C.; Caron, B.; Botuha, C.; Karaiskou, A.; Salmain, M.; Sobczak-Thépot, J. Cytotoxic BODIPY-Appended Half-Sandwich Iridium(III) Complex Forms Protein Adducts and Induces ER Stress. *J. Med. Chem.* **2021**, *64*, 16675−16686.
(9) Neuditschko, B.; Legin, A. A.; Baier, D.; Schintlmeister, A.; Reipert, S.; Wagner, M.; Keppler, B. K.; Berger, W.; Meier-Menches, S. M.; Gerner, C. Die Wechselwirkung mit ribosomalen Proteinen begleitet die Stressinduktion des Wirkstoffkandidaten BOLD-100/KP1339 im endoplasmatischen Retikulum. *Angew. Chem.* **2021**, *133*, 5121−5126.
(10) (a) Vidimar, V.; Meng, X.; Klajner, M.; Licona, C.; Fetzer, L.; Harlepp, S.; Hébraud, P.; Sidhoum, M.; Sirlin, C.; Loeffler, J. P.; Mellitzer, G.; Sava, G.; Pfeffer, M.; Gaiddon, C. Induction of caspase 8 and reactive oxygen species by ruthenium-derived anticancer compounds with improved water solubility and cytotoxicity. *Biochem Pharmacol.* **2012**, *84*, 1428−1436. (b) Xu, H. G.; Schikora, M.; Sisa, M.; Daum, S.; Klemt, I.; Janko, C.; Alexiou, C.; Bila, G.; Bilyy, R.; Gong, W.; Schmitt, M.; Sellner, L.; Mokhir, A. An Endoplasmic Reticulum Specific Pro-amplifier of Reactive Oxygen Species in Cancer Cells. *Angew. Chem., Int. Ed.* **2021**, *60*, 11158−11162.
(11) Dougan, S. J.; Habtemariam, A.; McHale, S. E.; Parsons, S.; Sadler, P. J. Catalytic organometallic anticancer complexes. *Proc. Natl. Acad. Sci. U.S.A.* **2008**, *105* (33), 11628−11633.
(12) Banerjee, S.; Dixit, A.; Shridharan, R. N.; Karande, A. A.; Chakravarty, A. R. *Endoplasmic reticulum*targeted chemotherapeutics: the remarkable photo-cytotoxicity of an oxovanadium(iv) vitamin-B6 complex in visible light. *Chem. Commun.* **2014**, *50*, 5590−5592.
(13) Goswami, T. K.; Gadadhar, S.; Balaji, B.; Gole, B.; Karande, A. A.; Chakravarty, A. R. Ferrocenyl-L-amino acid copper(II) complexes showing remarkable photo-induced anticancer activity in visible light. *Dalton Trans.* **2014**, *43*, 11988−11999.
(14) (a) Nam, J. S.; Kang, M. G.; Kang, J.; Park, S. Y.; Lee, S. J.; Kim, H. T.; Seo, J. K.; Kwon, O. H.; Lim, M. H.; Rhee, H. W.; Kwon, T. H. Endoplasmic Reticulum-Localized Iridium(III) Complexes as Efficient Photodynamic Therapy Agents via Protein Modifications. *Chem. Soc.* **2016**, *138*, 10968−10977. (b) Yuan, B.; Liu, J.; Guan, R.; Jin, C.; Ji, L.; Chao, H. Endoplasmic reticulum targeted cyclometalated iridium(iii) complexes as efficient photodynamic therapy photosensitizers. *Dalton Trans.* **2019**, *48*, 6408−6415.
(15) Tripathy, S. K.; De, U.; Dehury, N.; Laha, P.; Panda, M. K.; Kim, H. S.; Patra, S. Cyclometallated iridium complexes inducing paraptotic cell death like natural products: synthesis, structure and mechanistic aspects. *Dalton Trans.* **2016**, *45*, 15122−15136.
(16) (a) Cortez, L.; Sim, V. The therapeutic potential of chemical chaperones in protein folding diseases. *Prion* **2014**, *8*, 197−202. (b) Perlmutter, D. H. Chemical chaperones: a pharmacological strategy for disorders of protein folding and trafficking. *Pediatr. Res.* **2002**, *52*, 832−836.
(17) (a) Di, J.; Siddique, I.; Li, Z.; Malki, G.; Hornung, S.; Dutta, S.; Hurst, I.; Ishaaya, E.; Wang, A.; Tu, S.; Boghos, A.; Ericsson, I.; Klärner, F. G.; Schrader, T.; Bitan, G. The molecular tweezer CLR01 improves behavioral deficits and reduces tau pathology in P301S-tau transgenic mice. *Alzheimer's Res. Ther.* **2021**, *13*, 6. (b) Bengoa-Vergniory, N.; Faggiani, E.; Ramos-Gonzalez, P.; Kirkiz, E.; Connor-Robson, N.; Brown, L. V.; Siddique, I.; Li, Z.; Vingill, S.; Cioroch, M.; Cavaliere, F.; Threlfell, S.; Roberts, B.; Schrader, T.; Klärner, F. G.; Cragg, S.; Dehay, B.; Bitan, G.; Matute, C.; Bezard, E.; Wade-Martins, R. CLR01 protects dopaminergic neurons in vitro and in mouse models of Parkinson's disease. *Nat. Commun.* **2020**, *11*, 4885. (c) Herrera-Vaquero, M.; Bouquio, D.; Kallab, M.; Biggs, K.; Nair, G.; Ochoa, J.; Heras-Garvin, A.; Heid, C.; Hadrovic, I.; Poewe, W.; Wenning, G. K.; Klärner, F. G.; Schrader, T.; Bitan, G.; Stefanova, N. The molecular tweezer CLR01 reduces aggregated, pathologic, and seeding-competent α-synuclein in experimental multiple system atrophy. *Biochim. Biophys. Acta, Mol. Basis Dis.* **2019**, *1865*, 165513.
(18) Özcan, U.; Yilmaz, E.; Özcan, L.; Furuhashi, M.; Vaillancourt, E.; Smith, R. O.; Görgün, C. Z.; Hotamisligil, G. S. Chemical chaperones reduce ER stress and restore glucose homeostasis in a mouse model of type 2 diabetes. *Science* **2006**, *313*, 1137−1140.
(19) (a) Herzog, G.; Shmueli, M. D.; Levy, L.; Engel, L.; Gazit, E.; Klärner, F. G.; Schrader, T.; Bitan, G.; Segal, D. The Lys-Specific Molecular Tweezer, CLR01, Modulates Aggregation of the Mutant p53 DNA Binding Domain and Inhibits Its Toxicity. *Biochemistry* **2015**, *54*, 3729−3738. (b) Sinha, S.; Lopes, D. H.; Du, Z.; Pang, E. S.; Shanmugam, A.; Lomakin, A.; Talbiersky, P.; Tennstaedt, A.; McDaniel, K.; Bakshi, R.; Kuo, P. Y.; Ehrmann, M.; Benedek, G. B.; Loo, J. A.; Klärner, F. G.; Schrader, T.; Wang, C.; Bitan, G. Lysine-specific molecular tweezers are broad-spectrum inhibitors of assembly and toxicity of amyloid proteins. *J. Am. Chem. Soc.* **2011**, *133*, 16958−16969.
(20) Siepi, M.; Politi, J.; Dardano, P.; Amoresano, A.; De Stefano, L.; Maria Monti, D.; Notomista, E. Modified denatured lysozyme effectively solubilizes fullerene c60 nanoparticles in water. *Nanotechnology* **2017**, *28*, 335601.
(21) Jafvert, C. T.; Kulkarni, P. P. Buckminsterfullerene's (C60) octanol-water partition coefficient (Kow) and aqueous solubility. *Sci. Technol.* **2008**, *42*, 5945−5950.
(22) (a) Meng, J.; Liang, X.; Chen, X.; Zhao, Y. Biological characterizations of [Gd@C82(OH)22]n nanoparticles as fullerene derivatives for cancer therapy. *Integr. Biol.* **2013**, *5*, 43−47. (b) Lin, J.; Cai, R.; Sun, B.; Dong, J.; Zhao, Y.; Miao, Q.; Chen, C. Gd@$C_{82}(OH)_{22}$ harnesses inflammatory regeneration for osteogenesis of mesenchymal stem cells through JNK/STAT3 signaling pathway. *J. Mater. Chem. B* **2018**, *6*, 5802−5811.
(23) (a) Voloshin, Y. Z.; Kostromina, N. A.; Krämer, R.; *Clathrochelates: Synthesis, Structure and Properties*; Elsevier Science, 2002. (b) Voloshin, Y.; Belaya, I.; Krämer, R. *Cage Metal Complexes: Clathrochelates Revisited*; Springer, 2017.

https://doi.org/10.1021/jacs.3c08827
J. Am. Chem. Soc. XXXX, XXX, XXX−XXX

(24) Kovalska, V.; Chernii, S.; Cherepanov, V.; Losytskyy, M.; Chernii, V.; Varzatskii, O.; Naumovets, A.; Yarmoluk, S. The impact of binding of macrocyclic metal complexes on amyloid fibrillization of insulin and lysozyme. *J. Mol. Recognit.* **2017**, *30*, No. e2622.
(25) Kovalska, V. B.; Losytskyy, M. Y.; Varzatskii, O. A.; Cherepanov, V. V.; Voloshin, Y. Z.; Mokhir, A.; Yarmoluk, S. M.; Volkov, S. V. Study of anti-fibrillogenic activity of iron(II) clathrochelates. *Bioorg. Med. Chem.* **2014**, *22*, 1883−1888.
(26) Blechinger, J.; Varzackii, O. A.; Kovalska, V.; Zelinskii, G. E.; Voloshin, Y. Z.; Kinski, E.; Mokhir, A. Cytotoxicity of electrophilic iron(II)−clathrochelates in human promyelocytic leukemia cell line. *Med. Chem. Lett.* **2016**, *26*, 626−629.
(27) Belov, A. S.; Belaya, I. G.; Novikov, V. V.; Starikova, Z. A.; Polshin, E. V.; Dolganov, A. V.; Lebed, E. G. Structure, spectral and electrochemical properties of the 2,6-di-tert-butylphenol-functionalized iron and cobalt(ii) clathrochelates and their phenylsulfide analogs. *Inorg. Chim. Acta* **2013**, *394*, 269−281.
(28) Selin, R.; Chornenka, N.; Chernii, V. Ya.; Mokhir, A.; Vologzhanina, A. V.; Belov, A. S.; Pomadchik, A. L.; Voloshin, Y. Z. Chemical design of the heterodifunctionalized iron(II) clathrochelates with terminal biorelevant carboxyl group and reactive triple C≡C bond: Synthesis, structure, redox properties and their stability in various media. *Inorg. Chim. Acta* **2019**, *496*, 119047.
(29) Selin, R.; Klemt, I.; Chernii, V. Ya.; Losytskyy, M. Yu.; Chernii, S.; Mular, A.; Gumienna-Kontecka, E.; Kovalska, V. B.; Voloshin, Y. Z.; Vologzhanina, A. V.; Dorovatovskii, P. V.; Mokhir, A. Synthesis and spectral characterization of the first fluorescein-tagged iron(ii) clathrochelates, their supramolecular interactions with globular proteins, and cellular uptake. *RSC Adv.* **2021**, *11*, 8163−8177.
(30) Coan, K. E.; Maltby, D. A.; Burlingame, A. L.; Shoichet, B. K. Promiscuous aggregate-based inhibitors promote enzyme unfolding. *J. Med. Chem.* **2009**, *52*, 2067−2075.
(31) (a) Shen, D.; Coleman, J.; Chan, E.; Nicholson, T. P.; Dai, L.; Sheppard, P. W.; Patton, W. F. Novel Cell- and Tissue-Based Assays for Detecting Misfolded and Aggregated Protein Accumulation Within Aggresomes and Inclusion Bodies. *Cell Biochem. Biophys.* **2011**, *60*, 173−185. (b) Beriault, D. R.; Werstuck, G. H. Detection and quantification of endoplasmic reticulum stress in living cells using the fluorescent compound, Thioflavin T. *Biochim. Biophys. Acta* **2013**, *1833*, 2293−2301.
(32) Rooney, J. P.; Chorley, B.; Hiemstra, S.; Wink, S.; Wang, X.; Bell, D. A.; van de Water, B.; Corton, J. C. Mining a human transcriptome database for chemical modulators of NRF2. *PLoS* **2020**, *15*, No. e0239367.
(33) Ríos, N.; Prolo, C.; Álvarez, M. N.; Piacenza, L.; Radi, R. Peroxynitrite Formation and Detection in Living Cells. *Nitric Oxide Biology and Pathobiology*; Academic Press, 2017; pp 271−288.
(34) Santos, C. X.; Tanaka, L. Y.; Wosniak, J.; Laurindo, F. R. Mechanisms and implications of reactive oxygen species generation during the unfolded protein response: roles of endoplasmic reticulum oxidoreductases, mitochondrial electron transport, and NADPH oxidase. *Antioxid. Redox Signaling* **2009**, *11*, 2409−2427.
(35) Daum, S.; Reshetnikov, M. S. V.; Sisa, M.; Dumych, T.; Lootsik, M. D.; Bilyy, R.; Bila, E.; Janko, C.; Alexiou, C.; Herrmann, M.; Sellner, L.; Mokhir, A. Lysosome-Targeting Amplifiers of Reactive Oxygen Species as Anticancer Prodrugs. *Angew. Chem., Int. Ed.* **2017**, *56*, 15545−15549.
(36) Reshetnikov, V.; Daum, S.; Janko, C.; Karawacka, W.; Tietze, R.; Alexiou, C.; Paryzhak, S.; Dumych, T.; Bilyy, R.; Tripal, P.; Schmid, B.; Palmisano, R.; Mokhir, A. ROS-Responsive N-Alkylaminoferrocenes for Cancer-Cell-Specific Targeting of Mitochondria. *Angew. Chem., Int. Ed.* **2018**, *57*, 11943−11946.
(37) Han, C.; Jin, L.; Mei, Y.; Wu, M. Endoplasmic reticulum stress inhibits cell cycle progression via induction of p27 in melanoma cells. *Cell Signal* **2013**, *25*, 144−149.
(38) Ma, Y.; Hendershot, L. M. The role of the unfolded protein response in tumour development: friend or foe? *Nat. Rev. Cancer* **2004**, *4*, 966−977.
(39) Wang, H.; Li, Y.; Wang, Y.; Han, Z. G.; Cai, B. C9orf100, a new member of the Dbl-family guanine nucleotide exchange factors, promotes cell proliferation and migration in hepatocellular carcinoma. *Mol. Med. Rep.* **2012**, *5*, 1169−1174.
(40) Guo, C.; Liu, S.; Wang, J.; Sun, M. Z.; Greenaway, F. T. ACTB in cancer. *Clin. Chim. Acta* **2013**, *417*, 39−44.
(41) Özkan, H. G.; Thakor, V.; Xu, H. G.; Bila, G.; Bilyy, R.; Bida, D.; Böttcher, M.; Mougiakakos, D.; Tietze, R.; Mokhir, A. Anticancer Aminoferrocene Derivatives Inducing Production of Mitochondrial Reactive Oxygen Species. *Chem.—Eur. J.* **2022**, *28*, No. e202104420.
(42) Bříza, T.; Rimpelová, S.; Králová, J.; Záruba, K.; Kejík, Z.; Ruml, T.; Martásek, P.; Král, V. Pentamethinium fluorescent probes: The impact of molecular structure on photophysical properties and subcellular localization. *Dyes Pigm.* **2014**, *107*, 51−59.
(43) Chazotte, B. Labeling mitochondria with TMRM or TMRE. *Cold Spring Harb. Protoc.* **2011**, *2011*, 895−897.

https://doi.org/10.1021/jacs.3c08827
J. Am. Chem. Soc. XXXX, XXX, XXX−XXX